

A New Candidate Structure of the H₂-PRE Phase of Solid Hydrogen

Tom Ichibha^{†*}

Materials Science and Technology Division, Oak Ridge National Laboratory, Oak Ridge, Tennessee 37831, USA

Yunwei Zhang[†]

School of Physics, Sun Yat-sen University, Guangzhou 510275, China and
Cavendish Laboratory, University of Cambridge, Cambridge CB30HE, United Kingdom

Kenta Hongo

Research Center for Advanced Computing Infrastructure,
JAIST, Asahidai 1-1, Nomi, Ishikawa 923-1292, Japan

Ryo Maezono[‡]

School of Information Science, JAIST, Nomi, Ishikawa 923-1292, Japan

Fernando A. Reboredo[§]

Materials Science and Technology Division, Oak Ridge National Laboratory, Oak Ridge, Tennessee 37831, USA
(Dated: January 3, 2022)

Experimental progress finally reached the metallic solid hydrogen phase, which was predicted by Wigner and Huntington over 80 years ago. However, the different structures in the phase diagram are still been debated due to the difficulty of diffraction experiments for high-pressured hydrogen. The determination of crystal structures under extreme condition is both of the basic condensed matter physics, and in planetary science: the behavior of giant gaseous planets (e.g. Jupiter, Saturn...) strongly depends on the properties of inner high-pressured hydrogen. This work describes new possible structures appearing under high pressures of 400~600 GPa. We applied a structural search using particle swarm optimization with density functional theory (DFT) to propose several candidate structures. For these structures, we performed fixed-node diffusion Monte Carlo simulations combined with DFT zero-point energy corrections to confirm their relative stability. We found $P2_1/c-8$ as a promising candidate structure for the H₂-PRE phase. $P2_1/c-8$ is predicted the most stable at 400 and 500 GPa. $P2_1/c-8$ reproduces qualitatively the IR spectrum peaks observed in the H₂-PRE phase. ^a

I. INTRODUCTION

Dense hydrogen undergoes phase transitions to solid crystals under high pressure, providing a variety of solid structural phases. At the lowest pressure, hydrogen assumes a hexagonal lattice of molecules with sufficient internal degrees of freedom to rotate each molecule (phase I) [1]. At around 110 GPa, the rotation freezes to a uniform orientation (phase II) [1]. At higher pressures, Raman and infrared (IR) spectrum experiments have revealed the existence of six distinct structural phases (Phases III [2], IV, IV' [3–5], V [5], H₂-PRE [6], and metallic hydrogen (MH) [7–9]). (Table I of [6] provides a complete summary of the structural phases and transition

pressures. However, another experimental work [9] proposed another phase diagram, which does not include the H₂-PRE phase.) However, it is technically difficult to identify the structural characteristics of these phases using X-ray or neutron diffraction experiments [1]. Hence, elucidation of these structures has been left as an important mission for electronic structure calculations.

Pioneering work [10], molecular dynamics simulation at a fixed pressure [11] at the phase-III range (>150GPa), was performed to predict the $Cmca-4$ structure. Subsequently, an *ab initio* random-search simulation (AIRSS) [12] was applied to find several additional candidate structures for phase III. Although this included the $Cmca-4$ structure, it was claimed that $C2/c-24$ was most likely, because its Raman spectrum was found to well-reproduce the experimentally observed frequencies [12]. Subsequent AIRSS investigations have reported more energetically stable structure than $C2/c-24$: a hexagonal $P6_122$ appearing at a phase-III pressure range (>150GPa) [13]. The Raman spectrum of the $P6_122$ structure is consistent with experimental observations [13]. Further experimental investigations on the pressure dependence of the spectrum [14] has revealed a structural transition at around 190 GPa. Powder X-ray diffraction experiments have confirmed that this transition is accompanied by the deformation of an HPC-like structure, which is consistent with theoretical predictions regarding the transition from $P6_122$ →

* ichibha@icloud.com

[†] These two authors made the same contribution.

[‡] rmaezono@me.com

[§] reboredofa@ornl.gov

^a This manuscript has been authored by UT-Battelle, LLC, under contract DE-AC05-00OR22725 with the US Department of Energy (DOE). The US government retains and the publisher, by accepting the article for publication, acknowledges that the US government retains a nonexclusive, paid-up, irrevocable, worldwide license to publish or reproduce the published form of this manuscript, or allow others to do so, for US government purposes. DOE will provide public access to these results of federally sponsored research in accordance with the DOE Public Access Plan (<http://energy.gov/downloads/doe-public-access-plan>).

$C2/c-24$ (deformed from six-fold symmetry) [13]. A structure originally found as a candidate structure of the phase III, $Cmca-12$ [12], was also recently focused on as a candidate structure of the H_2 -PRE phase [6]. This phase was observed between the Phases III and MH [6]. The transition pressures are 360 and 495 GPa [6]. The $Cmca-12$ structure was predicted the most stable from 424(3) to 447(3) GPa by quantum Monte Carlo, between the candidate structures of phases III and MH [15]. In addition, the IR spectrum of $Cmca-12$ qualitatively agrees with the experiment [6, 12].

While the phases I–III, H_2 -PRE, and MH are stable down to near 0 K, the phases IV and IV' are stable around or above room temperature [3, 4]. The transition from phases III to IV occurs around 220 GPa [3]. From the Raman spectrum, the structure of phase IV was expected to be a mixed structure of atomic and molecular crystals. It was also found that the band gap and the Raman spectrum showed discontinuous behaviors at 275 GPa, implying a phase transition from IV to IV' [4]. AIRSS was used to predict phases IV and IV'. Phase IV was proposed to be a mixed structure ($Pc-48$), where two inequivalent layers alternatively appear. One layer is formed by strongly-bound molecules, and the other layer is formed by a graphene-like array of atomic hydrogen[16]. This mixed structure was found to be energetically more stable than others proposed thus far at room temperature in the range of 250 ~ 295 GPa [16]. The computed Raman spectrum of the structure was also found to be consistent with experiments [16].

TABLE I. Most promising candidates of each structural phase.

Phase	Structure	Description	Reference
II	$P2_1/c$	HCP ^a of molecules	[12]
	$P6_3/m$	HCP ^a of molecules	[12]
III (LP) ^b	$P6_122$	layered molecular	[13]
III (HP) ^c	$C2/c-24$	layered molecular	[12]
IV/IV'	$Pc-48$	mixed crystal	[16]
V	$Pca2_1$	mixed crystal	[17]
H_2 -PRE	$Cmca-12$	molecular crystal	[12, 15]

^a hexagonal close-packed

^b low pressure side of phase III

^c high pressure side of phase III

By further increasing the pressure at room temperature, another phase V structure was discovered under ~325 GPa [5]. Its Raman spectrum suggests that the band gap shrinks while the molecules are dissociated as the pressure increases. Therefore, this phase was considered as a stepping stone to the MH phase. The spectrum cannot be explained by any of the proposed structures at that time, stimulating further structural searches beyond the harmonic approximation [17]. The anharmonic approach [17] was then used to discover a new $Pca2_1$ structure, which provided a spectrum that was consistent with the experiments. The structure consists of hydrogen molecules with longer bond lengths that lead to narrower band gaps, which are consistent with the features experimentally captured in phase V. Table I summarizes the most promising

candidates, in our view, of each structural phase predicted theoretically.

In this study, we perform a structural search at zero temperature in a high-pressure region (400 ~ 600 GPa), where a structure has yet to be determined by experiments. By using the particle-swarm optimization (PSO) algorithm implemented in CALYPSO [18, 19], we found 10 new candidate structures beyond those reported in existent publications ($C2/c-24$ [12], $Cmca-12$ [12], $Cmca-4$ [10, 12], $I4_1/amd$ [20], and $mC-24$ [21]). For these candidates, we performed fixed-node diffusion Monte Carlo (FNDMC) calculations [22]. FNDMC includes many body corrections beyond DFT, to obtain static formation enthalpies. This reliable framework has been already applied in several previous solid hydrogen publications [15, 17, 23–26]. Note that, in addition, other QMC methods (i.e., path integral and reptation QMC) have been also utilized to study the properties of fluid hydrogen [27–32].

Among the structures found by structural search, $Pbam-8$ is predicted by FNDMC to have a static enthalpy comparable with the structures reported in the previous studies as shown in Table I. However $Pbam-8$ has imaginary frequency phonons which signals a structural instability. Therefore, we relax the structure along the direction of the imaginary mode and obtain a slightly different structure, $P2_1/c-8$. We find that $P2_1/c-8$ has the lowest dynamic enthalpy at zero temperature and at 400 GPa and 500 GPa. The dynamic enthalpy is given as the sum of the zero-point energy (ZPE) predicted by DFT and FNDMC static enthalpy. Therefore, we propose $P2_1/c-8$ to be a new candidate structure of the H_2 -PRE phase [6]. We confirm that the IR spectrum of $P2_1/c-8$ qualitatively agrees with the experiment for the H_2 -PRE phase, as well as the conventional candidate, $Cmca-12$ [6].

II. METHODS

A PSO structural search using CALYPSO [18, 19] is performed under 400 GPa with different unit-cell sizes comprising 2 to 70 atoms. Forty structures are generated with every iteration, and 30 % of the structures are generated using the artificial bee-colony algorithm [33] according to the structures appearing in the prior iteration; however, the remaining 70 % are generated randomly. We run 45 iterations for every unit-cell size. We use the Perdew–Burke–Ernzerhof (PBE) DFT method implemented in the Vienna Ab initio Simulation Package (VASP) [34] for geometric optimization and energy evaluation. Ionic cores are represented by projector-augmented wave pseudo potentials [35]. The cutoff energy (E_{cut}) for the plane wave basis set is chosen as 700 eV on the k -mesh for the integration over the Brillouin zone with a mesh size $< 0.30 \text{ \AA}^{-1}$. The threshold for self-consistent field (SCF) convergence is taken as 1.0×10^{-5} eV. Structural relaxations are performed until the total energy converges within the threshold: 1.0×10^{-5} eV.

On obtaining candidate structures using CALYPSO, we replace the exchange-correlation (XC) functionals into Van

der Waals (vdW) density functionals (DFs) [36] to perform additional structural relaxations at 400, 500, and 600 GPa using VASP [34] with $E_{\text{cut}} = 1,500$ eV and k -mesh sizes as $< 0.25 \text{ \AA}^{-1}$, which are the conditions needed to achieve total energy convergence within 0.1 mHartree/atom for the $I4_1/amd$ structure. SCF convergences are achieved using tighter thresholds of 1.0×10^{-6} eV, and the relaxations are performed until the force field at each ion falls to within 1.0×10^{-3} eV/Å.

ZPE is evaluated using the frozen phonon scheme implemented in Phonopy [37] coupled with VASP as the DFT kernel under the same computational conditions mentioned above. We take the simulation cell size to be larger than 72 f.u., for which the finite size error of ZPE is confirmed to be less than 0.1 mHartree/atom for the $I4_1/amd$ structure. We also confirm that the ZPE hardly depends on the functional. In addition to vdW-DF, we perform PBE [38] to evaluate the ZPE, finding that their difference are just 0.03 mHartrees in the case of $I4_1/amd$. We used Phonopy-Spectroscopy to calculate IR spectrum [39].

We evaluate FNDMC static enthalpies using QMCPACK [40]. Ionic cores are represented by the effective core potential developed for FNDMC calculations [41]. Our fixed-node trial wave function is a Slater–Jastrow type [22], wherein orbital functions used to form the determinant are generated by DFT with vdW-DF functionals [36] implemented in Quantum Espresso [42]. The cutoff energy is 300 Ry, for which the total energies of $C2/c-24$ and $I4_1/amd$ converge to within 0.04 mHartree/atom. The Jastrow function consists of the one-, two- and three-body terms, amounting to 78 variational parameters. The parameters are optimized using the linear method [43] implemented in QMCPACK. We use a simulation cell comprising ~ 100 atoms for FNDMC calculations to suppress the two-body finite size error. We also apply the kinetic energy correction [44] and the model periodic Coulomb interaction [45–47]. We use twist-averaged boundary conditions [48] with a $5 \times 5 \times 5$ twist-grid, with which the total energies of $C2/c-24$ and $I4_1/amd$ are converged to within 0.1 mHartree/atom. The timestep of FNDMC calculation is 0.02 a.u. $^{-1}$, with which the total energies of $C2/c-24$ and $I4_1/amd$ converge to within 0.05 mHartree/atom. For all FNDMC calculations, the target population is set to 1,024. The random walkers evolve during equilibration and statistical accumulation steps of 2,000 and 48,000, respectively.

In FNDMC, forces are practical for only simple small systems due to the computational cost. The second derivatives of energy are much more difficult so they are not implemented yet in QMCPACK to our knowledge. Without a Hessian, we cannot calculate phonons. Therefore, we rely in DFT methods to obtain geometry and phonons in this work. We note that, to our knowledge, there is only one example of FNDMC phonon calculation for diamond [49] using TurboRVB [50].

For fairness of comparison with other studies, we do not perform volume optimization at the FNDMC level. An additional $P \cdot V$ term in the static enthalpy is evaluated by the $V(P)$ dependence using DFTs at $P = 400, 500$, and 600 GPa. By

adding ZPE, we obtain dynamic enthalpies.

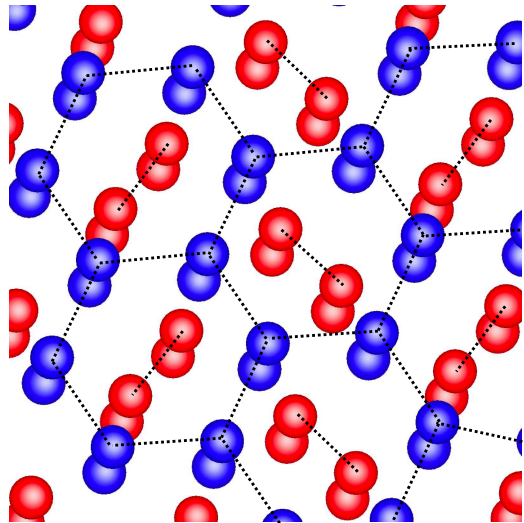


FIG. 1. The crystal structure of *Pbam-8*. Hydrogen molecules with very short bond lengths are located with their axes vertical to the layer. The layers formed by the blue molecules and red ones are alternately stacked. Although the blue layer forms a honeycomb lattice, the molecules in the red layer are ordered such that each pair accommodated within the honeycomb cell is defined by two adjacent blue layers flanking the red one.

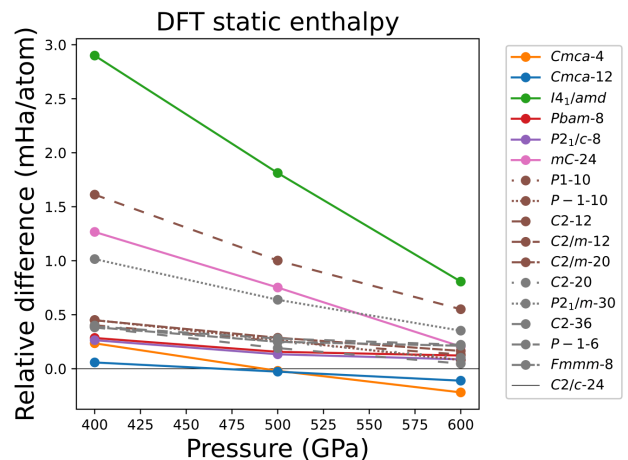


FIG. 2. Comparisons of static enthalpies evaluated by DFT in terms of the difference from the $C2/c-24$ structure (zero reference in the plot). The most stable structure is found to be $C2/c-24 \rightarrow Cmca-12 \rightarrow Cmca-4$ as pressure increases. Figure 3 shows more reliable prediction of static enthalpies by FNDMC.

III. RESULTS AND DISCUSSIONS

Using the PSO structural search, we find 10 new candidate structures beyond those reported in preceding works ($C2/c-24$, $Cmca-12$, $Cmca-4$, $I4_1/amd$, and $mC-24$). Comparisons

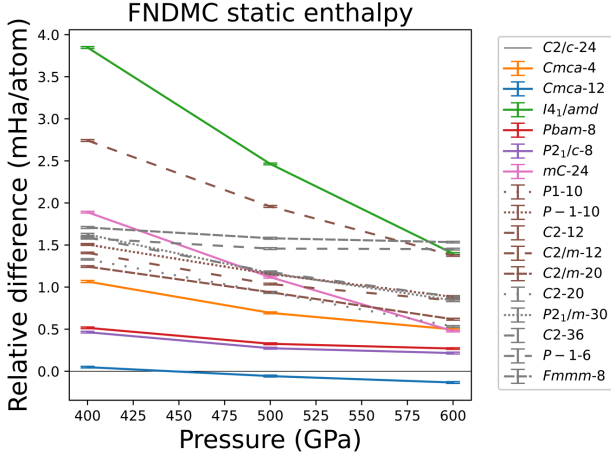


FIG. 3. Comparisons of static enthalpies evaluated by FNDMC in terms of the difference from the $C2/c-24$ structure (zero reference in the plot). Statistical error bars are shown. Figure 7 shows dynamic enthalpies calculated as the sum of this FNDMC static enthalpies and DFT ZPE shown in Figure 8.

of their static enthalpies predicted by vdW-DF functional are shown in Fig. 2. The 10 structures include nine molecular crystals and one mixed structure, $Pbam-8$. $Pbam-8$ comprises of atomic and molecular crystal layers appearing alternatively, as shown in Figure 1. The preceding PBE study [15, 21] reports that $mC-24$ (quasi-molecular) and $I4_1/amd$ (atomic) structures have the lowest static enthalpy under pressures higher than ~ 500 GPa. In contrast, these structures are evaluated as being relatively unstable in our vdW-DF results, as shown in Figure 2. McMinis *et al.* compare static enthalpies using both vdW-DF and PBE, reporting that atomic crystals, $I4_1/amd$ and β -Sn, are more unstable than molecular crystals, $C2c-24$, $Cmca-4$, and $Cmca-12$, when vdW-DF is applied [15]. Similarly, $mC-24$ (quasi-molecular) is likely to get unstable when vdW-DF is applied, as shown in the present work, owing to the longer molecular distances.

Figure 3 shows static enthalpies of structural phases predicted by FNDMC. However, the 10 structures are predicted to have negative phonons. Therefore, we tried to find a dynamically stable structure based on the phonon dispersion. Among the 10 structures we find, $Pbam-8$ has a notably low static enthalpy. $P2_1/c-8$ was found after relaxing $Pbam-8$ in the direction of instability. Figure 4 shows the phonon dispersion and phonon density of states (phonon DOS) of $Pbam-8$ at 400 GPa. There are imaginary modes around the Γ point and near the T point. We relax the structure along the direction of the imaginary mode at the Γ point and obtain a different structure, $P2_1/c-8$, as shown in Figure 5. Compared with $Pbam-8$, the hydrogen molecules are shifted out of a plane, as shown by arrows in Figure 5(a). The phonon dispersion and phonon DOS of $P2_1/c-8$ at 400 GPa are shown in Figure 6(a). $P2_1/c-8$ does not have negative phonons around the Γ point. We similarly try to relax $P2_1/c-8$ along the direction of the imaginary mode at T point. However, the re-

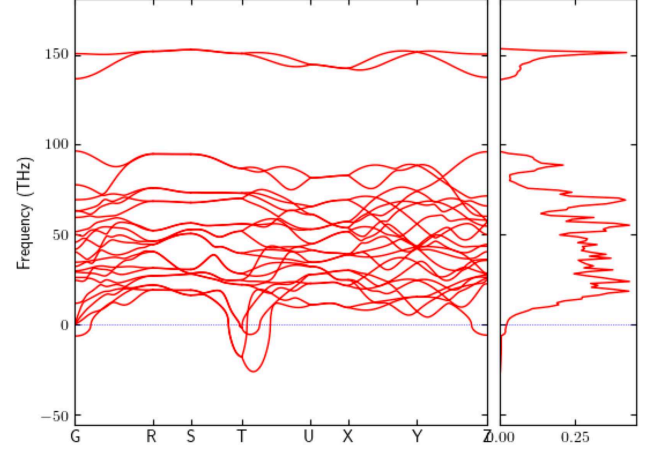


FIG. 4. Phonon dispersion of $Pbam-8$ structure at 400 GPa. The correspondences between labels and \vec{q} -points are G: $\vec{q}=(0,0,0,0,0)$, R: $\vec{q}=(0.5,0.5,0.5)$, S: $\vec{q}=(0.5,0.5,0,0)$, T: $\vec{q}=(0,0,0.5,0.5)$, U: $\vec{q}=(0.5,0,0,0.5)$, X: $\vec{q}=(0.5,0,0,0,0)$, Y: $\vec{q}=(0,0,0.5,0,0)$, and Z: $\vec{q}=(0,0,0,0,0.5)$.

laxed structure is identical to $P2_1/c-8$. We argue that small numerical errors in the harmonic finite difference approach implemented in Phonopy [37] or anharmonic effects might be responsible of those remaining imaginary frequency modes, since the structure is stable under deformation along those distortions. However, the population of imaginary modes in the harmonic phonon DOS is insignificant. Figure 6(b)(c) shows the phonon dispersion and phonon DOS of $P2_1/c-8$ at 500 and 600 GPa. The population of imaginary modes is negligible at 500 GPa but significantly large at 600 GPa, suggesting an instability there. Therefore, we calculated ZPE at 400 and 500 GPa only.

Fig. 7 shows the dynamic enthalpies (sum of the FNDMC static enthalpy; Fig. 3, and the ZPE calculated by DFT-phonon calculations (Fig. 8). Among the reported structures (*i.e.*, except for $P2_1/c-8$), the most stable structure changes as $C2/c-24 \rightarrow Cmca-12 \rightarrow I4_1/amd$. This result qualitatively agree with the previous FNDMC study [15]. Our newly found $P2_1/c-8$ structure is predicted more stable than the structures above at 400 and 500 GPa. Therefore, we propose $P2_1/c-8$ as the new candidate structure of the phase H_2 -PRE, which was experimentally found to exist from 360 to 495 GPa. The earlier candidate structure of H_2 -PRE, $Cmca-12$ [6, 12], no longer appears to be stable structure according to our calculations.

However, the difference of dynamic enthalpy between $P2_1/c-8$ and the second most stable structure is, at most, just 0.049(15) mHartree/atom. Therefore, $C2/c-24$ or $Cmca-12$ can be predicted comparably stable as $P2_1/c-8$, by taking into account anharmonic contributions to ZPE [17, 23, 24] or nuclear quantum effects [51], or using FNDMC forces [52, 53]. Nevertheless, $P2_1/c-8$ would remain among the most stable structures.

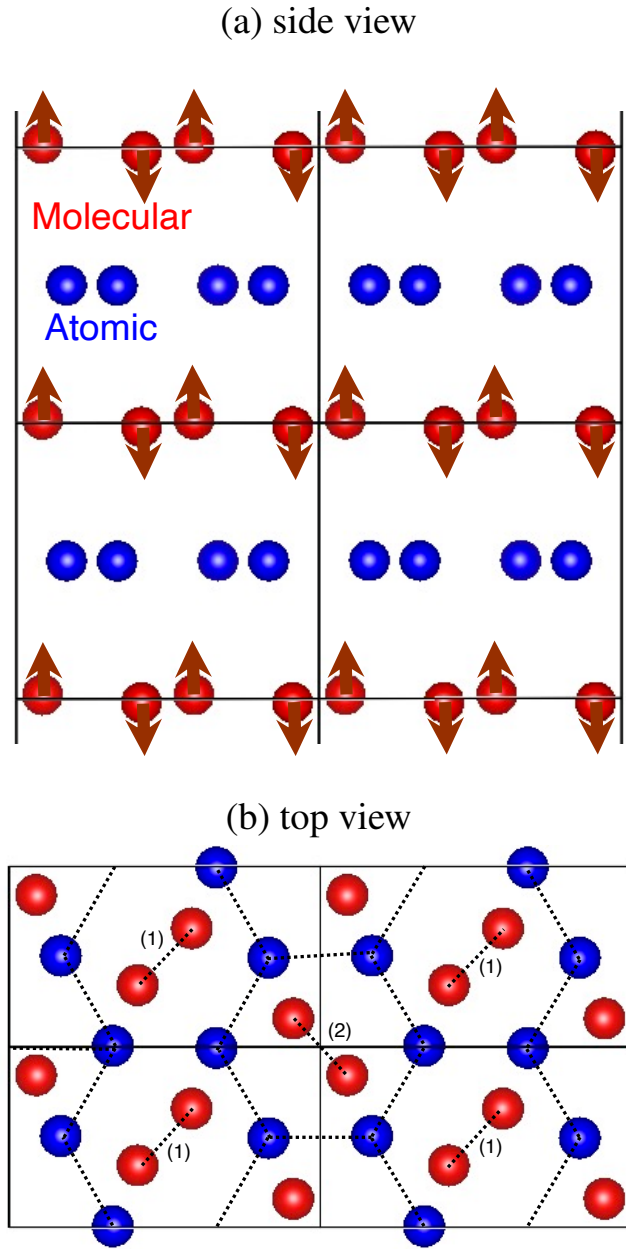


FIG. 5. Crystal structure of $P2_1/c-8$. The hydrogen atoms in the molecular (atomic) crystal layers are shown in red (blue). The arrows in the out-of-plane direction represent the shifts from $Pbam-8$.

IR spectrum measurements revealed that the H_2 -PRE phase has two peaks above 2800 cm^{-1} [6]. At 400 GPa, the peaks are at 2930 and 3264 cm^{-1} , which are taken from Figure 2 of Ref. 6 using WebPlotDigitizer [54]. Figure 9 shows our predicted IR spectra obtained for $P2_1/c-8$ and $Cmca-12$ structures with vdW-DF functional compared to the peaks observed experimentally [6]. $Cmca-12$ structure has two peaks around 4000 cm^{-1} in consistent with the previous theoretical works [55, 56]. Existence of the two peaks is a reason why $Cmca-12$ has been considered promising as the H_2 -PRE structure. Our $P2_1/c-8$ also has two peaks above 2000 cm^{-1} similar

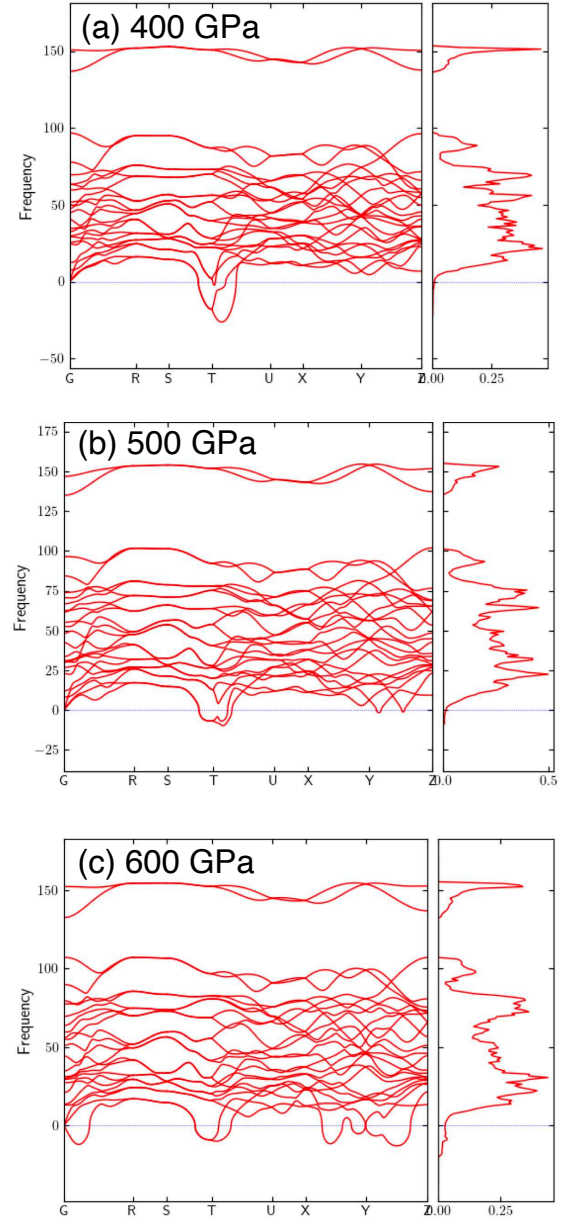


FIG. 6. Phonon dispersions of $P2_1/c-8$ structure at 400, 500, and 600 GPa. The correspondences between labels and \vec{q} -points are Γ : $\vec{q}=(0.0,0.0,0.0)$, R: $\vec{q}=(0.5,0.5,0.5)$, S: $\vec{q}=(0.5,0.5,0.0)$, T: $\vec{q}=(0.0,0.5,0.5)$, U: $\vec{q}=(0.5,0.0,0.5)$, X: $\vec{q}=(0.5,0.0,0.0)$, Y: $\vec{q}=(0.0,0.5,0.0)$, and Z: $\vec{q}=(0.0,0.0,0.5)$.

to $Cmca-12$ but with a lower formation energy. Therefore, we propose that $P2_1/c-8$ is a more promising candidate structure of the H_2 -PRE phase.

The structure of $P2_1/c-8$ is similar to $Pca2_1$ found as a candidate structure of the phase V [17]. The structure of $Pca2_1$ is shown in Figure 10. This structure consists of the hexagonal atomic crystal layers and the molecular layers, where the

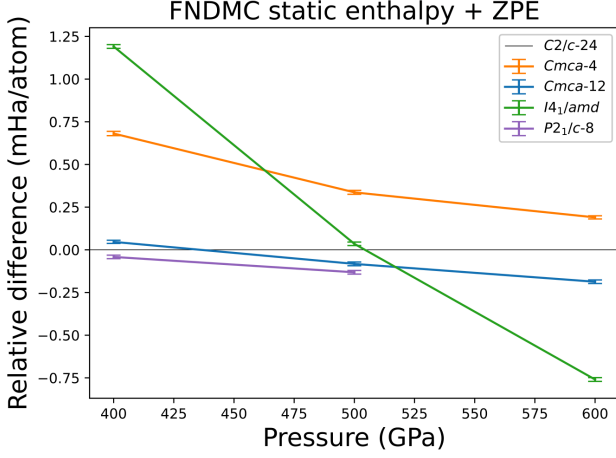


FIG. 7. Comparisons of dynamic enthalpies evaluated by FNDMC and DFT phonon evaluations in terms of the difference from the $C2/c-24$ structure (zero reference in the plot). This is the main result of this paper. Statistical error bars are shown.

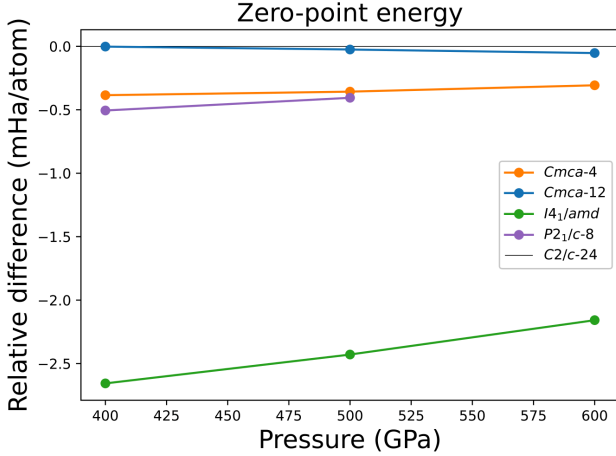


FIG. 8. Comparisons of DFT ZPE predicted by the phonon calculations in terms of the difference from the $C2/c-24$ structure (zero reference in the plot).

molecules are in the center of the hexagonal rings. The pronounced difference between $P2_1/c-8$ and $Pca2_1$ is the periodicity in the c -axis direction. Only for $Pca2_1$, the neighboring molecular layers are rotationally different by 180° around the c -axis. In addition, $P2_1/c-8$ is more symmetric also in the ab -plane direction than $Pca2_1$. In a molecular layer of a periodic cell, there are two types of molecular angles for $P2_1/c-8$ and eight types of molecular angles for $Pca2_1$. Over all, $P2_1/c-8$ structure is more translational symmetric than $Pca2_1$ structure. We discuss structural relationship between $P2_1/c-8$ and $C2/c-24$ or $I4_1/amd$ in the Appendix.

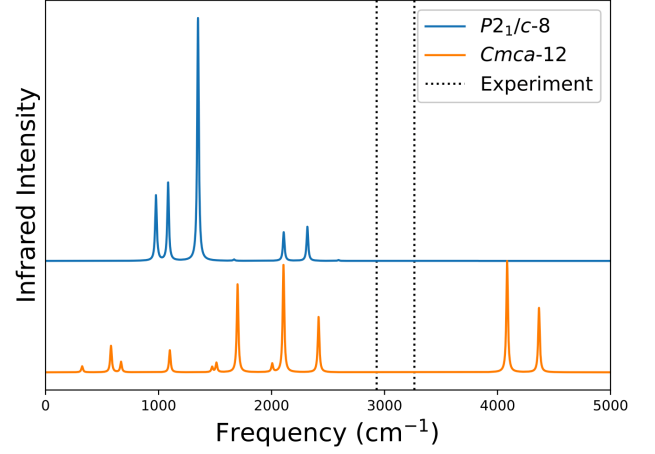


FIG. 9. The IR spectrum of $P2_1/c-8$ and $Cmca-12$ structures at 400 GPa. The vertical lines indicate the peaks found by the experiment [6].

IV. CONCLUSION

We performed a new structural search for solid-phase hydrogen at zero temperature in a high-pressure region, from 400 to 600 GPa. After obtaining candidate structures predicted using the PSO algorithm, we compared their enthalpies while considering the electron-correlation effects using the FNDMC method with zero-point energy corrections evaluated within the harmonic approximation of a phonon spectra. We found 10 candidate structures in our structural search. Among the structures, $Pbam-8$ is predicted to have a comparatively low static enthalpy by FNDMC with the previously reported structures. However, $Pbam-8$ has imaginary phonon modes. We relaxed the structure along the direction of the imaginary mode at the Γ point and obtained a new structure, $P2_1/c-8$. This structure has negligible population of imaginary modes at 400 and 500 GPa, which we attribute to numerical error or anharmonic effects. Our dynamic enthalpy evaluation given as the sum of the FNDMC static enthalpy and ZPE predicted by DFT showed that $P2_1/c-8$ is the most stable at 400 and 500 GPa. In addition, we found that the predicted IR spectrum of $P2_1/c-8$ qualitatively reproduces observed peaks for the pre-metallic phase, H_2 -PRE [6]. Therefore, we propose $P2_1/c-8$ as the new candidate structure of the H_2 -PRE phase, which was experimentally found to exist from 360 to 495 GPa [6].

V. APPENDIX

The structure of $P2_1/c-8$ is slightly similar to that of $C2/c-24$ found as a candidate structure of the phase III [12]. The structure of $C2/c-24$ is shown in Figure 11. The unit cell of $C2/c-24$ consists of four equivalent molecular layers with angular and translational differences. Each layer consists of distorted hexagonal lattices. Figure 11(b) shows only two neigh-

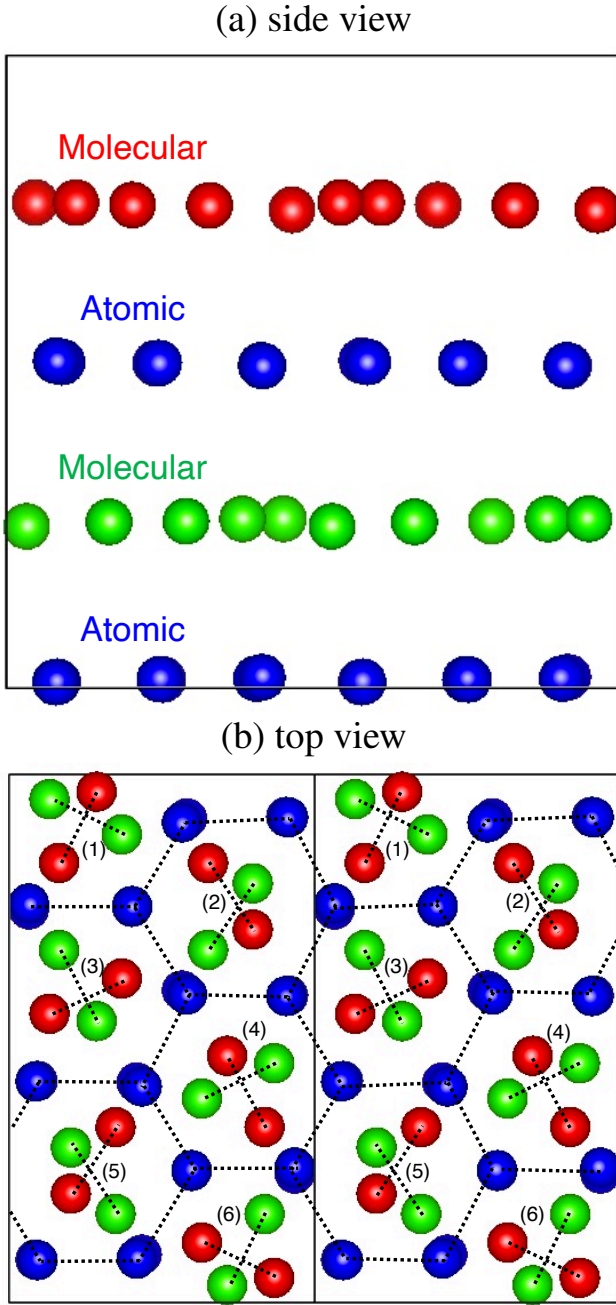


FIG. 10. Crystal structure of $Pca2_1$. The hydrogen atoms in the atomic crystal layers are shown in blue. The hydrogen atoms in the molecular crystal layers are shown in red or green. The red and green molecular layers are different by 180° around the c -axis.

boring layers. A molecule in the blue layer is located in the center of a distorted hexagonal lattice, similarly to $P2_1/c-8$. However, the molecule in the blue layer is also a member of a hexagonal lattice in the blue layer. Compared with $C2/c-24$, $P2_1/c-8$ is regarded that hydrogen atoms in one layer move to form strict hexagonal lattices and ones in another layer move to form isolated molecules. On the other hand, for a candidate structure of the metallic hydrogen, $I4_1/amd$, shown in Figure

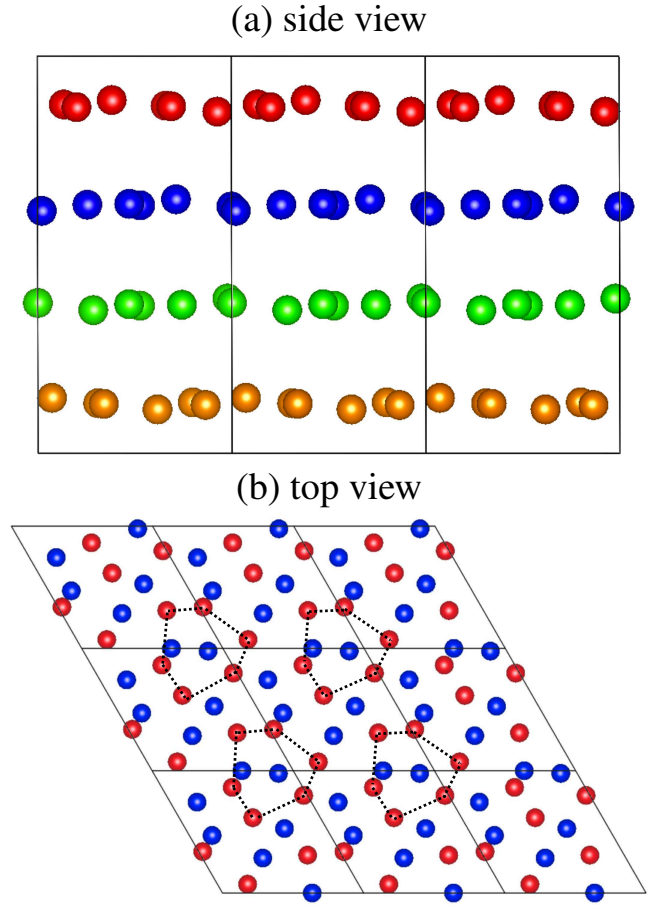


FIG. 11. Crystal structure of $C2/c-24$. Equivalent four layers are in a unit cell. They have angular and translational differences. Only the first and second layers are shown in the lower figure.

12 we cannot find any similarity with the other structures.

VI. ACKNOWLEDGMENTS

We thank Prof. Dr. Yanming Ma, Dr. Bartomeu Monserrat, and Dr. Kosuke Nakano for the useful discussions. We used VESTA [57] to draw the crystal structures. This work was supported by the US Department of Energy, Office of Science, Basic Energy Sciences, Materials Sciences and Engineering Division. We acknowledge computational resources provided by the Oak Ridge Leadership Computing Facility at Oak Ridge National Laboratory, which is a user facility of the Office of Science of the US Department of Energy under Contract No. DE-AC05-00OR22725, and by the Compute and Data Environment for Science (CADES) at Oak Ridge National Laboratory. We also acknowledge computational resources provided the Research Center for Advanced Computing Infrastructure (RCACI) at JAIST. T.I. is grateful for financial support from Grant-in-Aid for JSPS Research Fellow (18J12653). K.H. is grateful for financial support from MEXT-KAKENHI (JP16H06439, JP19K05029, JP19H05169, and JP21K03400), and the

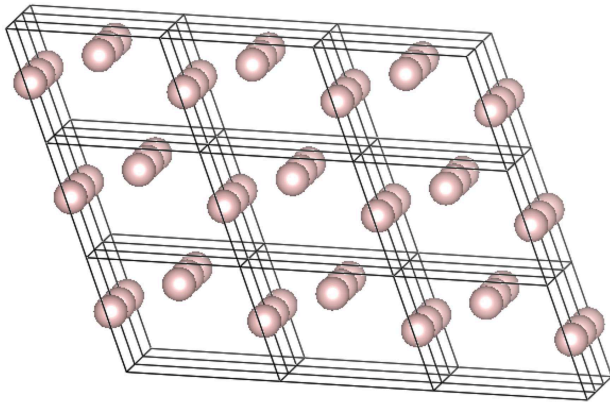


FIG. 12. Crystal structure of $I4_1/amd$.

Air Force Office of Scientific Research (Award Numbers: FA2386-20-1-4036). R.M. is grateful for financial supports from MEXT-KAKENHI (JP19H04692 and JP16KK0097), FLAGSHIP2020 (project nos. hp190169 and hp190167 at K-computer), the Air Force Office of Scientific Research (AFOSR-AOARD/FA2386-17-1-4049; FA2386-19-1-4015), and JSPS Bilateral Joint Projects (JPJSBP120197714).

-
- [1] P. Loubeyre, R. LeToullec, D. Hausermann, M. Hanfland, R. J. Hemley, H. K. Mao, and L. W. Finger, X-ray diffraction and equation of state of hydrogen at megabar pressures, *Nature* **383**, 702 (1996).
 - [2] H.-k. Mao and R. J. Hemley, Ultrahigh-pressure transitions in solid hydrogen, *Rev. Mod. Phys.* **66**, 671 (1994).
 - [3] R. T. Howie, C. L. Guillaume, T. Scheler, A. F. Goncharov, and E. Gregoryanz, Mixed molecular and atomic phase of dense hydrogen, *Phys. Rev. Lett.* **108**, 125501 (2012).
 - [4] R. T. Howie, T. Scheler, C. L. Guillaume, and E. Gregoryanz, Proton tunneling in phase iv of hydrogen and deuterium, *Phys. Rev. B* **86**, 214104 (2012).
 - [5] P. Dalladay-Simpson, R. T. Howie, and E. Gregoryanz, Evidence for a new phase of dense hydrogen above 325 gigapascals, *Nature* **529**, 63 (2016).
 - [6] R. P. Dias, O. Noked, and I. F. Silvera, Quantum phase transition in solid hydrogen at high pressure, *Phys. Rev. B* **100**, 184112 (2019).
 - [7] R. P. Dias, O. Noked, and I. F. Silvera, New phases and dissociation-recombination of hydrogen deuteride to 3.4 mbar, *Phys. Rev. Lett.* **116**, 145501 (2016).
 - [8] R. P. Dias and I. F. Silvera, Observation of the wigner-huntington transition to metallic hydrogen, *Science* **355**, 715 (2017).
 - [9] P. Loubeyre, F. Occelli, and P. Dumas, Synchrotron infrared spectroscopic evidence of the probable transition to metal hydrogen, *Nature* **577**, 631 (2020).
 - [10] K. A. Johnson and N. W. Ashcroft, Structure and bandgap closure in dense hydrogen, *Nature* **403**, 632 (2000).
 - [11] G. J. Martyna, D. J. Tobias, and M. L. Klein, Constant pressure molecular dynamics algorithms, *The Journal of Chemical Physics* **101**, 4177 (1994).
 - [12] C. J. Pickard and R. J. Needs, Structure of phase iii of solid hydrogen, *Nat. Phys.* **3**, 473 (2007).
 - [13] B. Monserrat, R. J. Needs, E. Gregoryanz, and C. J. Pickard, Hexagonal structure of phase iii of solid hydrogen, *Phys. Rev. B* **94**, 134101 (2016).
 - [14] Y. Akahama, Y. Mizuki, S. Nakano, N. Hirao, and Y. Ohishi, Raman scattering and x-ray diffraction studies on phase III of solid hydrogen, *Journal of Physics: Conference Series* **950**, 042060 (2017).
 - [15] J. McMinis, R. C. Clay, D. Lee, and M. A. Morales, Molecular to atomic phase transition in hydrogen under high pressure, *Phys. Rev. Lett.* **114**, 105305 (2015).
 - [16] C. J. Pickard, M. Martinez-Canales, and R. J. Needs, Density functional theory study of phase iv of solid hydrogen, *Phys. Rev. B* **85**, 214114 (2012).
 - [17] B. Monserrat, N. D. Drummond, P. Dalladay-Simpson, R. T. Howie, P. López Ríos, E. Gregoryanz, C. J. Pickard, and R. J. Needs, Structure and metallicity of phase v of hydrogen, *Phys. Rev. Lett.* **120**, 255701 (2018).
 - [18] Y. Wang, J. Lv, L. Zhu, and Y. Ma, Crystal structure prediction via particle-swarm optimization, *Phys. Rev. B* **82**, 094116 (2010).
 - [19] Y. Wang, J. Lv, L. Zhu, and Y. Ma, Calypso: A method for crystal structure prediction, *Computer Physics Communications* **183**, 2063 (2012).
 - [20] J. M. McMahon and D. M. Ceperley, Ground-state structures of atomic metallic hydrogen, *Phys. Rev. Lett.* **106**, 165302 (2011).
 - [21] H. Liu, H. Wang, and Y. Ma, Quasi-molecular and atomic phases of dense solid hydrogen, *The Journal of Physical Chemistry C* **116**, 9211 (2012).
 - [22] W. M. C. Foulkes, L. Mitás, R. J. Needs, and G. Rajagopal, Quantum monte carlo simulations of solids, *Rev. Mod. Phys.* **73**, 33 (2001).
 - [23] S. Azadi, B. Monserrat, W. M. C. Foulkes, and R. J. Needs, Dissociation of high-pressure solid molecular hydrogen: A quantum monte carlo and anharmonic vibrational study, *Phys. Rev. Lett.* **112**, 165501 (2014).
 - [24] N. D. Drummond, B. Monserrat, J. H. Lloyd-Williams, P. L.pez Ros, C. J. Pickard, and R. J. Needs, Quantum monte carlo study of the phase diagram of solid molecular hydrogen at extreme pressures, *Nat. Comm.* **6**, 7794 (2015).
 - [25] S. Azadi, G. H. Booth, and T. D. Kühne, Equation of state of atomic solid hydrogen by stochastic many-body wave function methods (2020), arXiv:2009.00709.
 - [26] D. M. Ceperley and B. J. Alder, Ground state of solid hydrogen at high pressures, *Phys. Rev. B* **36**, 2092 (1987).
 - [27] V. Gorelov, D. M. Ceperley, M. Holzmann, and C. Pierleoni, Electronic energy gap closure and metal-insulator transition in dense liquid hydrogen, *Phys. Rev. B* **102**, 195133 (2020).
 - [28] G. Rillo, M. A. Morales, D. M. Ceperley, and C. Pierleoni, Optical properties of high-pressure fluid hy-

- drogen across molecular dissociation, *Proceedings of the National Academy of Sciences* **116**, 9770 (2019), <https://www.pnas.org/content/116/20/9770.full.pdf>.
- [29] C. Pierleoni, G. Rillo, D. M. Ceperley, and M. Holzmann, Electron localization properties in high pressure hydrogen at the liquid-liquid phase transition by coupled electron-ion monte carlo, *Journal of Physics: Conference Series* **1136**, 012005 (2018).
- [30] M. A. Morales, J. M. McMahon, C. Pierleoni, and D. M. Ceperley, Nuclear quantum effects and nonlocal exchange-correlation functionals applied to liquid hydrogen at high pressure, *Phys. Rev. Lett.* **110**, 065702 (2013).
- [31] C. Pierleoni, M. Holzmann, and D. M. Ceperley, Local structure in dense hydrogen at the liquid-liquid phase transition by coupled electron-ion monte carlo, *Contributions to Plasma Physics* **58**, 99 (2017).
- [32] C. Pierleoni, M. A. Morales, G. Rillo, M. Holzmann, and D. M. Ceperley, Liquid-liquid phase transition in hydrogen by coupled electron-ion monte carlo simulations, *Proceedings of the National Academy of Sciences* **113**, 4953 (2016).
- [33] Q. Bian, Z. Yang, Y. Wang, C. Cao, and S. Pan, Predicting global minimum in complex beryllium borate system for deep-ultraviolet functional optical applications, *Scientific Reports* **6**, 34839 (2016), article.
- [34] G. Kresse and J. Furthmüller, Efficient iterative schemes for ab initio total-energy calculations using a plane-wave basis set, *Phys. Rev. B* **54**, 11169 (1996).
- [35] G. Kresse and D. Joubert, From ultrasoft pseudopotentials to the projector augmented-wave method, *Phys. Rev. B* **59**, 1758 (1999).
- [36] M. Dion, H. Rydberg, E. Schröder, D. C. Langreth, and B. I. Lundqvist, Van der waals density functional for general geometries, *Phys. Rev. Lett.* **92**, 246401 (2004).
- [37] A. Togo and I. Tanaka, First principles phonon calculations in materials science, *Scr. Mater.* **108**, 1 (2015).
- [38] J. P. Perdew, K. Burke, and M. Ernzerhof, Generalized Gradient Approximation Made Simple, *Phys. Rev. Lett.* **77**, 3865 (1996).
- [39] J. M. Skelton, L. A. Burton, A. J. Jackson, F. Oba, S. C. Parker, and A. Walsh, Lattice dynamics of the tin sulphides SnS_2 , SnS and SnS_3 : vibrational spectra and thermal transport, *Phys. Chem. Chem. Phys.* **19**, 12452 (2017).
- [40] J. Kim, A. D. Baczewski, T. D. Beaudet, A. Benali, M. C. Bennett, M. A. Berrill, N. S. Blunt, E. J. L. Borda, M. Casula, D. M. Ceperley, S. Chiesa, B. K. Clark, R. C. Clay, K. T. Delaney, M. Dewing, K. P. Esler, H. Hao, O. Heinonen, P. R. C. Kent, J. T. Krogel, I. Kylänpää, Y. W. Li, M. G. Lopez, Y. Luo, F. D. Malone, R. M. Martin, A. Mathuriya, J. McMinis, C. A. Melton, L. Mitas, M. A. Morales, E. Neuscamman, W. D. Parker, S. D. P. Flores, N. A. Romero, B. M. Rubenstein, J. A. R. Shea, H. Shin, L. Shulenburger, A. F. Tillack, J. P. Townsend, N. M. Tubman, B. V. D. Goetz, J. E. Vincent, D. C. Yang, Y. Yang, S. Zhang, and L. Zhao, {QMCPACK}: an open source ab initio quantum Monte Carlo package for the electronic structure of atoms, molecules and solids, *Journal of Physics: Condensed Matter* **30**, 195901 (2018).
- [41] A. Annaberdiyev, G. Wang, C. A. Melton, M. C. Bennett, L. Shulenburger, and L. Mitas, A new generation of effective core potentials from correlated calculations: 3d transition metal series, *The Journal of Chemical Physics* **149**, 134108 (2018).
- [42] P. Giannozzi, S. Baroni, N. Bonini, M. Calandra, R. Car, C. Cavazzoni, D. Ceresoli, G. L. Chiarotti, M. Cococcioni, I. Dabo, A. D. Corso, S. de Gironcoli, S. Fabris, G. Fratesi, R. Gebauer, U. Gerstmann, C. Gougoussis, A. Kokalj, M. Lazzeri, L. Martin-Samos, N. Marzari, F. Mauri, R. Mazzarello, S. Paolini, A. Pasquarello, L. Paulatto, C. Sbraccia, S. Scandolo, G. Sclauzero, A. P. Seitsonen, A. Smogunov, P. Umari, and R. M. Wentzcovitch, Quantum espresso: a modular and open-source software project for quantum simulations of materials, *Journal of Physics: Condensed Matter* **21**, 395502 (2009).
- [43] C. J. Umrigar, J. Toulouse, C. Filippi, S. Sorella, and R. G. Hennig, Alleviation of the fermion-sign problem by optimization of many-body wave functions, *Phys. Rev. Lett.* **98**, 110201 (2007).
- [44] S. Chiesa, D. M. Ceperley, R. M. Martin, and M. Holzmann, Finite-size error in many-body simulations with long-range interactions, *Phys. Rev. Lett.* **97**, 076404 (2006).
- [45] P. R. C. Kent, R. Q. Hood, A. J. Williamson, R. J. Needs, W. M. C. Foulkes, and G. Rajagopal, Finite-size errors in quantum many-body simulations of extended systems, *Phys. Rev. B* **59**, 1917 (1999).
- [46] L. M. Fraser, W. M. C. Foulkes, G. Rajagopal, R. J. Needs, S. D. Kenny, and A. J. Williamson, Finite-size effects and coulomb interactions in quantum monte carlo calculations for homogeneous systems with periodic boundary conditions, *Phys. Rev. B* **53**, 1814 (1996).
- [47] A. J. Williamson, G. Rajagopal, R. J. Needs, L. M. Fraser, W. M. C. Foulkes, Y. Wang, and M.-Y. Chou, Elimination of coulomb finite-size effects in quantum many-body simulations, *Phys. Rev. B* **55**, R4851 (1997).
- [48] C. Lin, F. H. Zong, and D. M. Ceperley, Twist-averaged boundary conditions in continuum quantum monte carlo algorithms, *Phys. Rev. E* **64**, 016702 (2001).
- [49] K. Nakano, T. Morresi, M. Casula, R. Maezono, and S. Sorella, Atomic forces by quantum monte carlo: Application to phonon dispersion calculations, *Phys. Rev. B* **103**, L121110 (2021).
- [50] K. Nakano, C. Attaccalite, M. Barborini, L. Capriotti, M. Casula, E. Coccia, M. Dagrada, C. Genovese, Y. Luo, G. Mazzola, A. Zen, and S. Sorella, Turborvb: A many-body toolkit for ab initio electronic simulations by quantum monte carlo, *The Journal of Chemical Physics* **152**, 204121 (2020), <https://doi.org/10.1063/5.0005037>.
- [51] M. A. Morales, J. M. McMahon, C. Pierleoni, and D. M. Ceperley, Towards a predictive first-principles description of solid molecular hydrogen with density functional theory, *Phys. Rev. B* **87**, 184107 (2013).
- [52] K. Nakano, A. Raghav, and S. Sorella, Space-warp coordinate transformation for efficient ionic force calculations in quantum monte carlo (2021), arXiv:2110.12234.
- [53] J. Tiihonen, R. C. Clay, and J. T. Krogel, Toward quantum monte carlo forces on heavier ions: Scaling properties, *The Journal of Chemical Physics* **154**, 204111 (2021), <https://doi.org/10.1063/5.0052266>.
- [54] A. Rohatgi, Webplotdigitizer: Version 4.5 (2021).
- [55] S. Azadi and W. M. C. Foulkes, Fate of density functional theory in the study of high-pressure solid hydrogen, *Phys. Rev. B* **88**, 014115 (2013).
- [56] C. J. Pickard, M. Martinez-Canales, and R. J. Needs, Density functional theory study of phase iv of solid hydrogen, *Phys. Rev. B* **85**, 214114 (2012).
- [57] K. Momma and F. Izumi, VESTA3 for three-dimensional visualization of crystal, volumetric and morphology data, *Journal of Applied Crystallography* **44**, 1272 (2011).